Subglacial landforms beneath Rutford Ice Stream, Antarctica: detailed bed topography from ice-penetrating radar.

E.C. King, H.D. Pritchard and A.M Smith

British Antarctic Survey

Abstract

We present a digital elevation model of the bed of Rutford Ice Stream, Antarctica derived from radio-echo sounding data. The data cover an 18 x 40 km area immediately upstream of the grounding line of the ice stream. This area is of particular interest because repeated seismic surveys have shown that rapid erosion and deposition of subglacial sediments has taken place. The bed topography shows a range of different subglacial landforms including mega-scale glacial lineations, drumlins and hummocks. This dataset will form a baseline survey which, when compared to future surveys, should reveal how active subglacial landscapes change over time. These data also allow comparison between subglacial landforms in an active system with those observed in deglaciated areas in both polar regions. The dataset comprises observed ice thickness data, an interpolated bed elevation grid, observed surface elevation data and a surface elevation grid. The dataset is available at http://doi.org/269

Introduction

Subglacial bedforms develop where ice flows over a sedimentary substrate, but precisely how this happens is still the subject of much research e.g.(Clark, 2010, Menzies, 1989, Rose, 1987, Fowler, 2010). The size and shape of large numbers of palaeo landforms have been mapped from exposed former ice sheet beds by satellite, airborne and shipboard systems e.g. (Clark and others, 2009,

Greenwood & Clark, 2010, Spagnolo and others, 2012) but accessing the bed of contemporary ice sheets for such studies is extremely difficult. While the basal topography beneath the Antarctic Ice Sheet is becoming better known at a spatial resolution of kilometres (Fretwell and others, 2013), there have been only a small number of surveys that provide spatial resolution of several metres that are hence capable of showing the size and distribution of sub-glacial landforms (King and others, 2009, King and others, 2007). These surveys have so far concentrated on Rutford Ice Stream, West Antarctica.

Rutford Ice Stream drains ice from the region of the Ellsworth Mountains into the Ronne Ice Shelf (Fig. 1) (King, 2009). In common with other ice streams, the surface slopes along the ice stream are low, which means the basal driving stress is low. Therefore, in order to flow at circa 400 m a^{-1} the resistance to flow provided by the bed must also be low (MacAyeal and others, 1995, Joughin and others, 2004). This implies the widespread presence of soft, unconsolidated, water-saturated sediments at the bed. Such sediments were first confirmed beneath Rutford Ice Stream using seismic surveying (Smith, 1997b, Smith & Murray, 2009), which also showed that the sediments were formed into elongate bedforms. The dataset presented by King and co-authors (King and others, 2009) used ice-penetrating radar to extend the mapping around the seismic lines to identify a suite of Mega-Scale Glacial Lineations (MSGLs). While extensive areas of MSGLs have been mapped in formerly glaciated areas (e.g. (Stokes & Clark, 2002), (Storrar & Stokes, 2007, Larter and others, 2009)), this was the first time MSGLs were mapped beneath actively-flowing ice at a similar 3D resolution to offshore swath bathymetry. That dataset was extended in the 2008-2009 Antarctic field season by further ground radar survey, covering an additional 25 km of the ice stream towards the grounding line. The combined dataset covers a 40 x 18 km section of the bed, representing about 20% of the fast-flowing part of the ice stream (that portion flowing at more than 100 m/a). In this paper, we present the combined dataset as a digital elevation model (DEM) of the bed which has grid dimensions of 100 x 25 m. The DEM provides the opportunity to compare the metrics of landforms beneath an active ice stream with those from palaeo ice stream beds, it also sets the context for more detailed seismic and radar studies of Rutford Ice Stream. The DEM will also act as a planning tool for bed-access drilling for sampling of substrate materials and measurement of basal conditions, as well as a baseline survey for the assessment of on-going erosion and deposition by repeat surveys in the future.

Location and previous work

Rutford Ice Stream has been the site of considerable investigation over the past three decades. The downstream portion of the ice stream occupies a 26 km wide, 2.4 km deep trough adjacent to the Ellsworth Mountains (Fig. 1). Repeated seismic reflection profiling (Smith, 1997a, Smith, 2007, Smith and others, 2007, Smith & Murray, 2009) showed that the bed of the ice stream is composed of a mixture of soft and stiff till; that the soft till was formed into elongate landforms; and that erosion and deposition of the basal sediment took place over short timescales. In one location (Fig. 1) an area 500 m across was eroded by 6 m in the 6 year interval between seismic surveys (Smith op cit), over the following 7 years a mound of sediment 100 m across and 10 m high was emplaced in the same location. In addition, the acoustic characteristics of sections of the till changed over the period indicating a transition from a soft, dilatant till to a stiff, lodged condition.

A radar survey of the bed topography surrounding the Smith (1997) seismic lines, revealed a large suite of drumlins and mega-scale glacial lineations (MSGLs) located in areas where the seismic surveys indicated soft, highly dilated, water-saturated sediment beneath the ice (King and others, 2009). Conversely, in areas where the seismic data indicated stiff till, the glacial landforms were much smaller, hummocky shapes. Over these hummocky areas, seismic recorders registered more micro earthquakes from the bed of the ice stream (indicative of stick-slip motion) than in areas where the soft, wet sediment was present (Smith, 2006), which were seismically 'quiet' (thought to equate to a more continuous style of movement due to the greater lubrication of the bed). This was a further indication that basal resistance to flow can vary spatially on a small scale, potentially leading to a shifting pattern of lubricated and sticky spots within the bed of the ice stream.

The ice surface flow velocity over the area of the radar survey is 365 m/a at the upstream end, accelerating to 400 m/a at the grounding line (Gudmundsson, 2006). There is a modulation of the flow speed at the grounding line of up to 20% with a fortnightly periodicity linked to the spring-neap tidal cycle(Gudmundsson, 2006). There was no significant variation in the flow speed of the ice stream over the 1979-2003 period (Gudmundsson & Jenkins, 2009).

Data acquisition, processing and visualisation

Acquisition

The bed elevation data were derived from ground-based radar surveys. The radar data were collected over two field seasons using the British Antarctic Survey's Deep Look Radio Echo Sounder (DELORES), operating at 3 MHz (King and others, 2009). This is a monopulse radar operating in the 1-

4 MHz range that is based on designs developed by the University of Washington (Gades, 1998) and St Olaf College (Welch & Jacobel, 2003). The transmitter fires a +/- 2500 V pulse into the antenna at a variable firing rate between 1 and 5 kHz. The antennae were resistively-loaded wire dipoles and the receiver used a chassis computer with a 100 MHz digitising card. The surveys reported here were acquired using 20 m half-dipole antennas which results in a centre frequency of approximately 3 MHz. The transmitter was fired at a pulse repetition rate of 1 kHz and 1000 shots were stacked in the oscilloscope buffer to form each recorded trace in order to improve the signal to noise ratio. A trigger pulse was transmitted between transmitter and the receiving digitiser via a fibre-optic cable. The radar equipment was towed behind a snowmobile travelling at about 12 km hr^{-1}, therefore each trace of the final record is built up of data acquired over a horizontal distance of circa 3m.

Each survey took a two-person team about three weeks to acquire. Navigation along the pre-planned lines was done using single-frequency GPS units mounted on the snowmobiles. A dual-frequency GPS receiver was operated on the recording sledge to provide accurate post-hoc positions. Lines were oriented orthogonal to the ice flow, spaced 500 m apart. Some lines were acquired parallel to ice flow in order to check for any triggering discrepancies that could induce time shifts in the picked bed profiles. Surface crevassing in the ice stream margins limited the lateral coverage and a zone of crevasses overlying the highest point in the bed topography resulted in a gap in coverage in the middle of the survey (Fig. 1).

Processing

The radar data were processed using ReflexW software (Sandmeier Scientific Software) in the following sequence:

- assign positioning information. The dual-frequency GPS data were processed using the kinematic-mode precise point positioning service provided by the Canadian Geodetic Service (http://webapp.geod.nrcan.gc.ca/geod/tools-outils/ppp.php). An offset was applied from the GPS antenna position (on the recording sledge) to the centre point of the antenna array to provide the geographic location of the reflection point on the bed.

- suppression of the effects of the direct (airwave + groundwave) arrival. The direct arrival is a very high amplitude pulse transmitted horizontally between the transmitting and receiving antennae. The effect on the receiving system is to induce 'wow' in the amplifier, that is a high-amplitude, very low frequency overprint on the

signal. Wow can be removed either by use of a frequency filter or by computing an average trace for the record and subtracting the average trace from each individual trace. The use of a bandpass filter on high amplitude signals can result in unwanted artefacts, particularly at the start and end of the record, so the average trace subtraction method was used here.

- bandpass filter. Frequencies below 0.5 MHz and above 10 MHz were suppressed to increase the signal-to-noise ratio.

- amplitude correction. The amplitudes were scaled proportional to the two-way travel time to compensate for the spherical spreading of the radar wave front.

- migration. The action of the migration step is to re-assign energy back to its source point, it has the effect of collapsing hyperbolae, correcting dipping events to true dip and improving horizontal resolution.

Figure 2a shows an example radar profile, displaying only that part of the record centred around the bed return. The display has high vertical exaggeration (7.5:1) to emphasise the shape of the landforms. The dominant event is the reflection from the bed of the ice stream. There is a very high degree of spatial correlation between each line (red lines in Fig. 2c).

The onset time of the bed reflection was determined at 7.5 m intervals along each line and converted to bed elevations with a precision of ±3 m. The bed is an interface with a much higher reflection coefficient than any near-by internal ice layers so the precision of the radar range measurement is not affected by ambiguity in resolving the bed reflection from other reflections. The criteria that determine the precision of the range measurement are the rise time of the source signal; the bandwidth of the system; and the digitisation interval. Here we assume that there is no change in the wave speed profile between two adjacent measurements. In our system the output voltage rises at 250V/ns, therefore the peak voltage is reached in 10 ns and the onset of the direct wave can be picked at the digital resolution which is 10 ns (i.e. the digitiser card samples the waveform at 10 ns intervals). The bandwidth of the recording system is 50 MHz with the result that reflections from high-contrast interfaces such as the bed have sharp onsets that can be easily picked for time of arrival. The remainder of the error budget for the bed elevation is made up of uncertainty in the GPS-derived elevation of the recording system and uncertainty in the depth-averaged wave velocity.

148 The horizontal resolution is a measure of the minimum size an object has to be to be
149 distinguishable as a separate entity on the target of interest. The size of the Fresnel zone at quarter-
150 wavelength is sometimes used as an estimate of horizontal resolution in radar data but that measure
151 is only valid for unmigrated data (see page 470 (Yilmaz, 1987)). Migration collapses the size of the
152 Fresnel zone to approximately one quarter of the dominant wavelength (Lindsey, 1989). Thus, the
153 theoretical horizontal resolution of these migrated data is given by:

154 $F_d = V_{avg}/4f$,

155 where F_d is the post-migration Fresnel diameter, V_{avg} is the average wave speed from surface
156 to bed and f is the frequency. For V_{avg} = 0.167 m ns^{-1} and the mean bandwidth frequency of 4.75
157 MHz, F_d = 8.8 m, comparable with the horizontal trace spacing of 7.5 m.

158 The final step in the processing sequence was to convert the processed radar data to SEG-Y
159 format to facilitate exchange of the data and import into interpretation software packages.

160 ***Picking the bed reflector and visualisation***

161 The processed radar data files were imported into the Petrel ™ Schlumberger interpretation
162 software package. The times of the reflections from the bed of the ice stream were picked on the
163 radar profiles using a semi-automatic picker that followed the peak of the reflection wavelet from
164 trace to trace. This created a raw dataset in *x,y,t* form where *x* and *y* were the coordinates in South
165 Polar Stereographic projection and *t* was the two-way travel time. The measured point values were
166 then interpolated onto a 25 m (cross-flow) x 100 m (along-flow) grid oriented orthogonal to the
167 profile lines using a natural neighbour algorithm with a 5:1 anisotropy ratio aligned along the ice
168 flow direction (Fig. 2c). This interpolation scheme preserves the continuity of features elongate in
169 the flow direction while preserving the high spatial sampling of the cross-flow bed profile.

170 The radar system determines the time-of-flight of the radio wave from the transmitter to the
171 receiver via a reflection from the bed. This information was converted into elevation of the bed with
172 respect to the WGS84 ellipsoid by using a time-to-depth conversion and then subtracting the depths
173 from the surface elevation as recorded by the dual-frequency GPS system mounted on the recording
174 sledge. The radar wave speed used for the time-to-depth conversion was 0.167 m.ns^{-1}. The use of a
175 single value of radar wave speed for the depth conversion is a simplification, it does not take into
176 account the variation in wave speed through the firn nor any variation with depth due to
177 temperature, though these variations are likely to change slowly in the horizontal direction. We are
178 not able to quantify these variations so the absolute elevations in the WGS84 ellipsoid reference

frame may be in error to the order of 10-20 m, even though the relative heights of the landforms are known to ± 3 m.

Limitations of the dataset

There is an implicit assumption in the acquisition and processing of single-source, single-receiver radar data that the reflection point lies vertically beneath the centre of the antenna array. This assumption is invalid under a number of circumstances, some of which can be corrected, others not. For reflection points that lie in the vertical plane through the profile line, reflections (or diffractions from point sources) can arise from points ahead of or behind the radar. Because the process of moving the system along the line renders these in-line but off-nadir reflections into hyperbolae on the record, they can be corrected during the migration processing step. However for reflection points lying off-nadir to either side of the line, it is not possible to reconstruct the original source point without additional cross-track records. Over large areas of the present survey this does not matter because the topography of the bed is largely two-dimensional and the line orientation was chosen to be orthogonal. The exceptions are areas where the bed slopes significantly in the in-flow direction, such as at the upstream or stoss end of drumlins, the upstream end of the Central High Ridge and the hummocky area in the centre of the survey. The effect is to limit the ability to accurately map the shape and position of the rounded ends of drumlins, even though the cross-profiles of the features is precisely known. We have conducted check surveys with closer cross-track spacing in some of the areas of potential uncertainty and find that the cross slopes are sufficiently shallow that side echoes do not map onto the in-line profile at times earlier that the vertical return from the bed.

The radar wave speed profile through the ice column is not known which means that values of ice thickness and therefore absolute bed elevation relative to sea level may have errors of circa 20 m, hence the adoption of a single value for the average wave speed. This uncertainty in the absolute elevation has no impact on the primary objective of the survey which was measurement and observation of subglacial landforms.

Results - map products

The bed elevation map is shown as Fig. 3, the same data, projected as a 3D view, is shown in Fig. 4. On the large scale the bed has a W profile with troughs to either side separated by a central

ridge. The central ridge is subdued in the upstream portion of the survey area (labelled 'Central Low Ridge' in Fig. 3 and much higher in the downstream portion ('Central High Ridge' in Fig. 3).

In order to emphasise the smaller scale landscape features we applied a high-pass spatial filter to the data and then subtracted the filtered data from the original. The 3D surface in Fig. 4 is colour-coded with the residual elevation to make the individual landforms more clearly distinguishable.

The curvature of the bed surface is shown in map form in Fig. 5. This display emphasises the difference between highly-elongate linear features with sharply-defined profiles, elongate but subdued features and subdued features with low elongation ratios. Curvature was calculated using a tool in ArcGIS that computes the second derivative value of the input surface on a cell-by-cell basis. A fourth-order polynomial is fit to a surface composed of a 3 x 3 window centred on the cell of interest, positive numbers indicate upward convexity, while negative numbers indicate upward concavity.

The surface elevation was derived from the dual-frequency GPS position information. Posted values at 7.5 m intervals along each survey line were used as input to create a surface model using convergent interpolation. The elevation in the upstream part of the survey is between 285 and 325 m above the WGS84 ellipsoid (Fig. 6), with no consistent downstream slope. A high point is reached near the centre of the survey which lies above the upstream end of the central ridge seen on the bed. The surface elevation downstream of this high point drops relatively steeply (by 70 m over 2 km) in the southeasterly direction.

There are several classes of subglacial bedform within the survey area (Fig. 7). A full description of the landforms will be presented elsewhere, here we summarise the main forms.

1.1. Parallel-sided MSGLs: The dominant features observed in the eastern trough are parallel-sided MSGLs which have large elongation ratios (i.e. great length, small width) and low amplitudes. These landforms are up to17 km long and are spaced an average of 300 to 400 m apart (Spagnolo et al 2014). In the NE trough, these features have a subtle kink in plan (Fig. 5), where they deviate toward the left (as viewed by an observer facing down flow) margin of the ice stream in the region of the step in the bed. Parallel-sided MSGL in the SW trough are continuous for about 16 km and terminate downstream at a sharply-defined line.

1.2. Tapering drumlins: There are 6 features which lie within the field of MSGLs but which are distinctly different. These have higher trough-to-crest amplitudes (up to 70 m); a crest line that rises steeply to a maximum near the upstream end then tapers slowly downstream. Usually the troughs to either side reach their lowest points adjacent to the highest point on the crest. The contrast between these features and the parallel-sided MSGLs is illustrated in Fig. 8 which shows portions of the bed elevation profiles picked from the radar profiles across part of the Central Ridge. The example drumlin tapers in width at each end and has much larger vertical relief than the adjacent MSGL.

1.3. Small drumlins or hummocks: the central and west-central parts of the survey are dominated by features with low amplitude and small elongation ratios (Fig.7). In the south-western trough there is a small group of drumlins that have higher amplitudes and longer elongation ratios but are distinct from the MSGLs and separated from them by a distinct boundary.

1.4. Other linear features: The high region in the south central part of the survey has few positive streamlined features , the linear features that do exist are mostly grooves. On the west flank of the topographic high there is a step approximately 40 m high which is oriented at an angle to the ice flow.

Parameters for the gridded dataset

Projection: Antarctic Polar Stereographic, WGS84 ellipsoid, Prime Meridian 0.0, Standard Parallel 71°S

Axis	*Min*	*Max*
X	-1299211.26	-1258669.79
Y	124167.22	154725.41
Depth [m] (below WGS84 ellipsoid)	-2185.76	-1476.94
Lat	78°23'51.3927"S	78°00'1.0350"S
Long	84°32'26.7107"W	82°59'30.9101"W
Increment in X-direction:	100	
Increment in Y-direction:	25	
Unrotated Xmin:	-1293677.31	
Unrotated Ymin:	124167.22	
Unrotated Xmax:	-1254477.31	

Unrotated Ymax:	143242.22	
Rotation angle:	18.6	
Number of 2D nodes in I-direction:	393	
Number of 2D nodes in J-direction:	764	
Topography Statistics		
Min:	-2185.76	m
Max:	-1476.94	m
Delta:	708.82	m
Number of defined values:	244280	
Mean:	-1858.71	m

260

261

262

Significance of the dataset

This dataset provides an extensive, high-resolution view of the landscape beneath an active ice stream. It will be of interest to those wishing to calibrate the palaeo record of ice stream tracks and to those seeking to understand the processes involved in generating subglacial landforms. All previous observations of fields of subglacial landforms have been from deglaciated regions, hence this dataset will enable the testing of theories concerning dewatering and sediment consolidation during the process of deglaciation. Given that repeat seismic surveys within the area have shown rapid rates of both erosion and deposition, this dataset forms a baseline survey for the assessment of sediment transport and landform evolution by way of repeat survey using similar techniques in the future. The dataset also allows the size and spatial distribution of landforms to be compared to the metrics of palaeo examples. The provision of the raw x,y,t picks in the dataset will facilitate precise re-survey and direct comparison of the raw data rather than the interpolated surfaces.

Data Access

The dataset (King and others, 2015) can be accessed at

http://doi.org/269

Acknowledgements

We gratefully acknowledge the field assistants, pilots and operations staff of the British Antarctic Survey's Rothera Station for their support during the field data collection. Schlumberger Plc is thanked for supplying educational licences for its Petrel software. This work was funded by BAS's Global Science in the Antarctic Context Programme (NERC award NE/B502287/1).

References

Clark, C.D. 2010. Emergent drumlins and their clones: from till dilatancy to flow instabilities. *J Glaciol*, **56**(200): 1011-1025.

Clark, C.D., A.L.C. Hughes, S.L. Greenwood, M. Spagnolo and F.S.L. Ng 2009. Size and shape characteristics of drumlins, derived from a large sample, and associated scaling laws. *Quaternary Science Reviews*, **28**(7-8): 677-692.

291 Fowler, A.C. 2010. The formation of subglacial streams and mega-scale glacial lineations. *P Roy Soc*
292 *a-Math Phy*, **466**(2123): 3181-3201.
293 Fretwell, P., H.D. Pritchard, D.G. Vaughan, J.L. Bamber, N.E. Barrand, R. Bell, C. Bianchi, R.G.
294 Bingham, D.D. Blankenship, G. Casassa, G. Catania, D. Callens, H. Conway, A.J. Cook, H.F.J.
295 Corr, D. Damaske, V. Damm, F. Ferraccioli, R. Forsberg, S. Fujita, Y. Gim, P. Gogineni, J.A.
296 Griggs, R.C.A. Hindmarsh, P. Holmlund, J.W. Holt, R.W. Jacobel, A. Jenkins, W. Jokat, T.
297 Jordan, E.C. King, J. Kohler, W. Krabill, M. Riger-Kusk, K.A. Langley, G. Leitchenkov, C.
298 Leuschen, B.P. Luyendyk, K. Matsuoka, J. Mouginot, F.O. Nitsche, Y. Nogi, O.A. Nost, S.V.
299 Popov, E. Rignot, D.M. Rippin, A. Rivera, J. Roberts, N. Ross, M.J. Siegert, A.M. Smith, D.
300 Steinhage, M. Studinger, B. Sun, B.K. Tinto, B.C. Welch, D. Wilson, D.A. Young, C. Xiangbin
301 and A. Zirizzotti 2013. Bedmap2: improved ice bed, surface and thickness datasets for
302 Antarctica. *Cryosphere*, **7**(1): 375-393.
303 Gades, A.M. 1998. Spatial and temporal variations of basal conditions beneath glaciers and ice
304 sheets inferred from radio echo soundings. (Ph. D. University of Washington.)
305 Greenwood, S.L. and C.D. Clark 2010. The sensitivity of subglacial bedform size and distribution to
306 substrate lithological control. *Sediment Geol*, **232**(3-4): 130-144.
307 Gudmundsson, G.H. 2006. Fortnightly variations in the flow velocity of Rutford Ice Stream, West
308 Antarctica. *Nature*, **444**(7122): 1063-1064.
309 Gudmundsson, G.H. and A. Jenkins 2009. Ice-flow velocities on Rutford Ice Stream, West Antarctica,
310 are stable over decadal timescales. *J. Glaciol.*, **55**(190).
311 Joughin, I., D.R. MacAyeal and S. Tulaczyk 2004. Basal shear stress of the Ross ice streams from
312 control method inversions. *Journal of Geophysical Research-Solid Earth*, **109**(B9).
313 King, E.C. 2009. Flow dynamics of the Rutford Ice Stream ice-drainage basin, West Antarctica, from
314 radar stratigraphy. *Annals of Glaciology*, **50**(51): 42-48.
315 King, E.C., R.C.A. Hindmarsh and C.R. Stokes 2009. Formation of mega-scale glacial lineations
316 observed beneath a West Antarctic ice stream. *Nature Geoscience*, **2**(8): 585-588.
317 King, E.C., H.D. Pritchard and A.M. Smith 2015. Rutford Ice Stream bed elevation DEM from radar
318 data. In Centre, P.D., *ed.*, Cambridge, UK.
319 King, E.C., J. Woodward and A.M. Smith 2007. Seismic and radar observations of subglacial bed
320 forms beneath the onset zone of Rutford Ice Stream Antarctica. *Journal of Glaciology*,
321 **53**(183): 665-672.
322 Larter, R.D., A.G.C. Graham, K. Gohl, G. Kuhn, C.D. Hillenbrand, J.A. Smith, T.J. Deen, R.A. Livermore
323 and H.W. Schenke 2009. Subglacial bedforms reveal complex basal regime in a zone of
324 paleo-ice stream convergence, Amundsen Sea embayment, West Antarctica. *Geology*, **37**(5):
325 411-414.
326 Lindsey, J.P. 1989. The Fresnel zone and its interpretive significance. *The Leading Edge*, **8**: 33-39.
327 MacAyeal, D.R., R.A. Bindschadler and T.A. Scambos 1995. Basal Friction of Ice-Stream-E, West
328 Antarctica. *J. Glaciol.*, **41**(138): 247-262.
329 Menzies, J. 1989. Drumlins - Products of Controlled or Uncontrolled Glaciodynamic Response. *Quat.*
330 *Sci. Rev.*, **8**(2): 151-158.
331 Rose, J. 1987. Drumlins as part of a glacier bedform continuum. In Menzies, J. and J. Rose, *eds.*
332 *Drumlin Symposium*, Rotterdam, Balkema, 360.
333 Smith, A.M. 1997a. Basal conditions on Rutford Ice Stream, West Antarctica, from seismic
334 observations. *Journal of Geophysical Research-Solid Earth*, **102**(B1): 543-552.
335 Smith, A.M. 1997b. Variations in basal conditions on Rutford ice stream, West Antarctica. *Journal of*
336 *Glaciology*, **43**(144): 245-255.
337 Smith, A.M. 2006. Microearthquakes and subglacial conditions. *Geophys. Res. Lett.*, **33**(24).
338 Smith, A.M. 2007. Subglacial bed properties from normal-incidence seismic reflection data. *Journal*
339 *of Environmental and Engineering Geophysics*, **12**(1): 3-13.

340 Smith, A.M. and T. Murray 2009. Bedform topography and basal conditions beneath a fast-flowing
341 West Antarctic ice stream. *Quaternary Science Reviews*, **28**(7-8): 584-596.
342 Smith, A.M., T. Murray, K.W. Nicholls, K. Makinson, G. Aoalgeirsdottir, A.E. Behar and D.G. Vaughan
343 2007. Rapid erosion, drumlin formation, and changing hydrology beneath an Antarctic ice
344 stream. *Geology*, **35**(2): 127-130.
345 Spagnolo, M., C.D. Clark and A.L.C. Hughes 2012. Drumlin relief. *Geomorphology*, **153**: 179-191.
346 Stokes, C.R. and C.D. Clark 2002. Are long subglacial bedforms indicative of fast ice flow? *Boreas*,
347 **31**(3): 239-249.
348 Storrar, R. and C.R. Stokes 2007. A Glacial Geomorphological Map of Victoria Island, Canadian Arctic.
349 *J Maps*: 191-210.
350 Welch, B.C. and R.W. Jacobel 2003. Analysis of deep-penetrating radar surveys of West Antarctica,
351 US-ITASE 2001. *Geophys. Res. Lett.*, **30**(8).
352 Yilmaz, O. 1987. *Seismic data processing.* Tulsa, Society of Exploration Geophysicists.

353

354

355 Figure Captions

356 1. Location map. Rutford Ice Stream flows towards the south east past the Ellsworth
357 Mountains at between 365 and 400 m a^{-1}. Radar survey lines shown in yellow. Lines
358 are spaced 500 m apart. Gaps in the coverage are due either to equipment failure or
359 the need to avoid crevasses. The grounding line is shown in green. Location of
360 profile line shown in Fig. 2 marked in red. Location of line C1 from Smith and Murray
361 (2009) shown in blue. Polar Stereographic Projection. Axes are kilometres from
362 South Pole.

363 2. Detail of radar data. a) Portion of radar profile across Rutford Ice Stream, windowed
364 around the ice/sediment interface. Insert shows a portion of the data before the
365 migration processing step. b) Close-up of interface reflection. The reflection is a
366 negative-positive-negative wavelet (white-black-white on the grey-scale record) with
367 a very high signal-to-noise ratio which allows very precise determination of the
368 travel time. c) 3D view of the data (red lines) and interpolated grid (black lines)
369 which shows the coherence of the picked data from line to line and shows that the
370 gridded data faithfully reproduce the observed data.

371 3. Map of bed elevation, referenced to the WGS84 ellipsoid. The difference between
372 the ellipsoid and mean sea level is not known in this region. The bed of the ice
373 stream has a W profile with a central ridge and troughs to either side. The
374 downstream portion of the central ridge is several hundred meters higher than the
375 surroundings and is likely to be a bedrock outcrop. Labels refer to features described
376 in the text.

377 4. 3D view of the gridded dataset. View is downstream towards the south east, vertical
378 exaggeration is approximately 10 to 1. The bed elevation surface has been colour-

coded by residual elevation to emphasise the landforms. Residual elevation was computed by differencing the bed elevation surface with a smoothed version which used a 2 km x 2 km spatial smoothing filter. Bold grid lines are spaced 4 km apart in the horizontal directions and 250 m apart in the vertical direction.

5. Map of the curvature of the bed elevation surface. This method of presenting the data emphasises the contrasts between high amplitude linear features, low amplitude linear features and low amplitude features with low elongation. Positive values of curvature indicate upward convexity and negative values upward concavity.

6. Map of the elevation of the surface of the ice stream referenced to the WGS84 ellipsoid. Data was collected using a dual-frequency GPS unit on the radar receiver sledge and post-processed using a kinematic technique (see text). Steepest surface slope occurs above the upstream end of the bedrock outcrop that forms the central high ridge at the bed.

7. Geomorphological interpretation. The features of the bed of the ice stream can be classified into a number of different landforms and surface features, based on amplitude, length, outline shape and whether they are positive or negative landscape elements. See text for full descriptions of each class.

8. Elevation profiles from the crest of the Central Low Ridge (Fig. 3) to illustrate the difference in cross-section between parallel-sided MSGLs (highlighted in green on the right hand panel) and tapering drumlins (highlighted in red). The drumlin tapers in width at both ends and has a maximum vertical relief an order of magnitude greater than the MSGL.

403

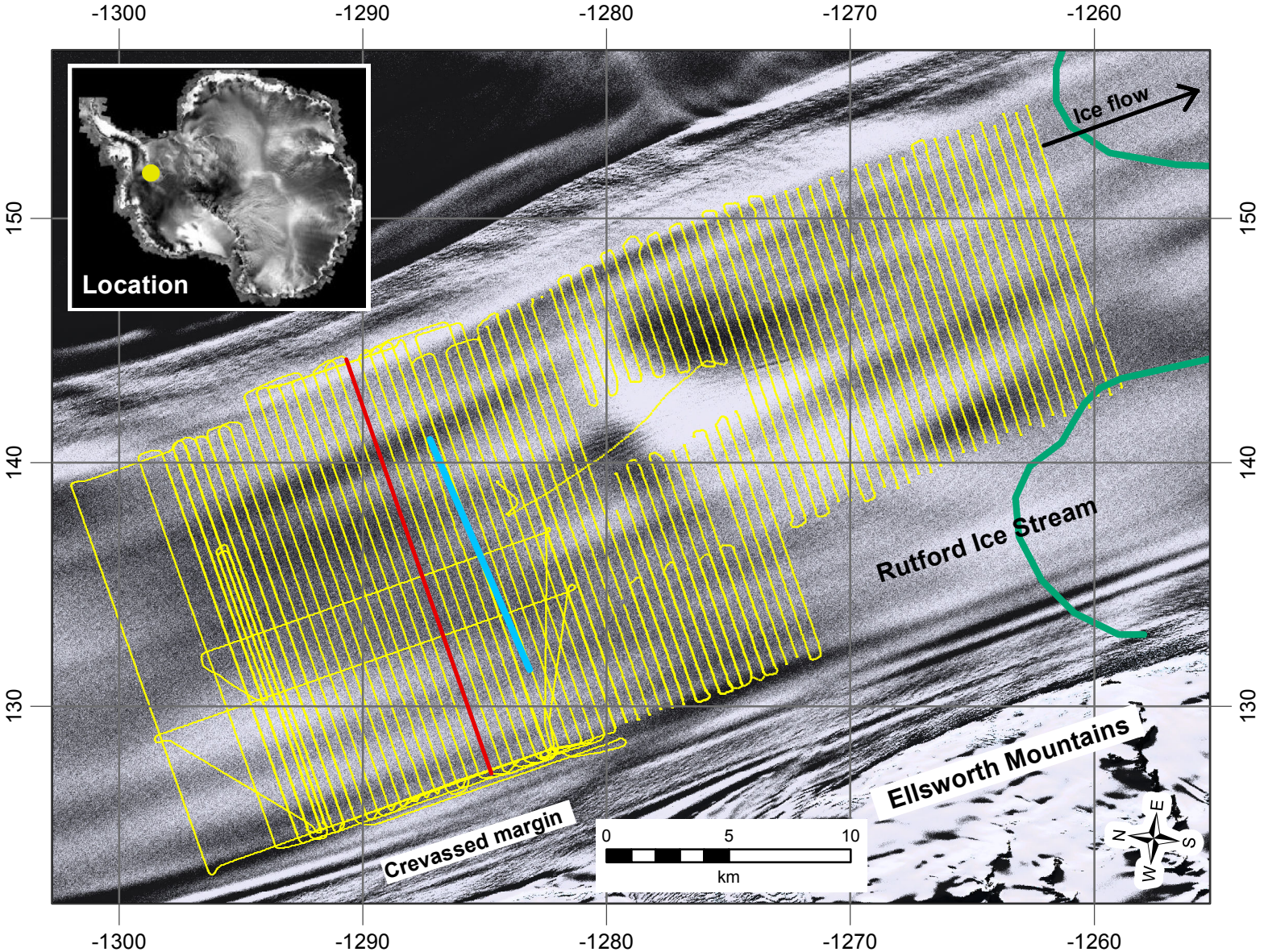

King et al Figure 1

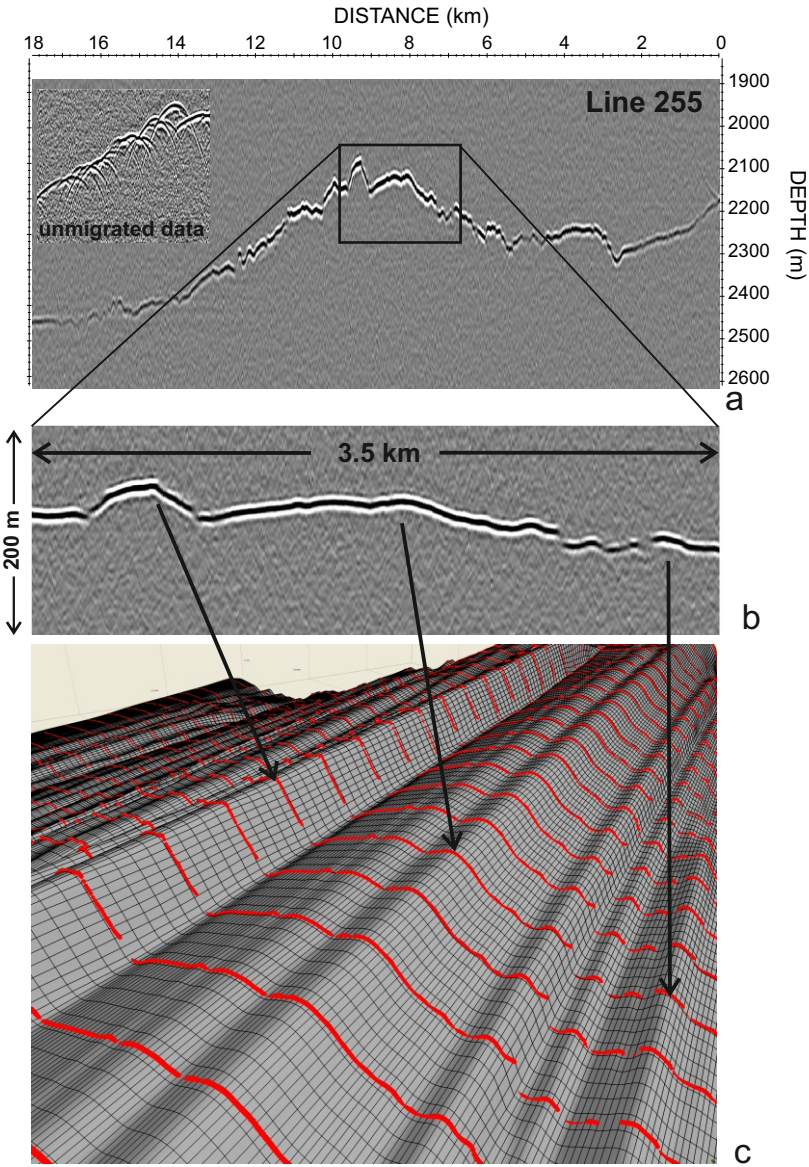

King et al Figure 2

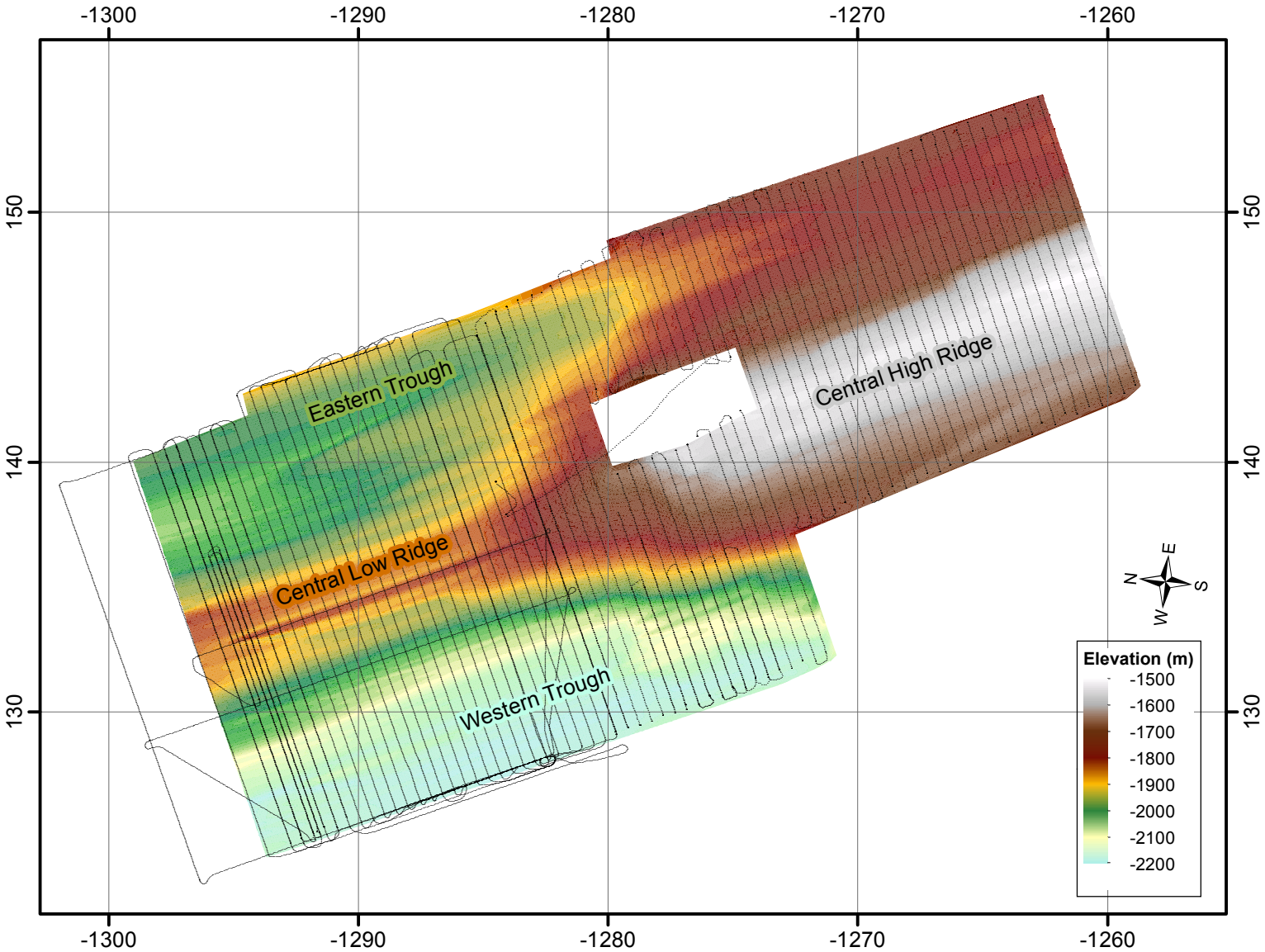

King et al Figure 3

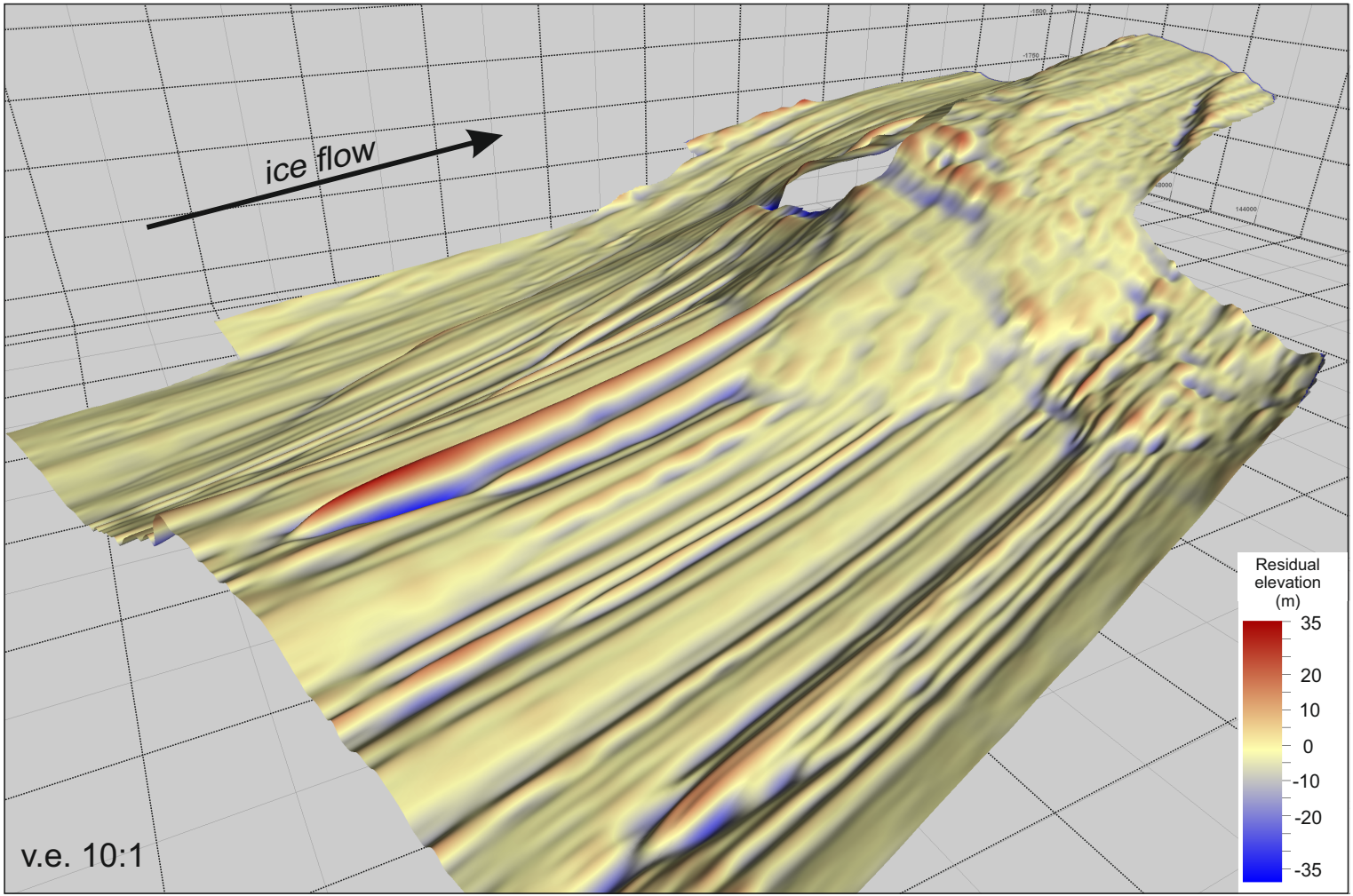
ice flow
v.e. 10:1
Residual elevation (m)
35
20
10
0
-10
-20
-35

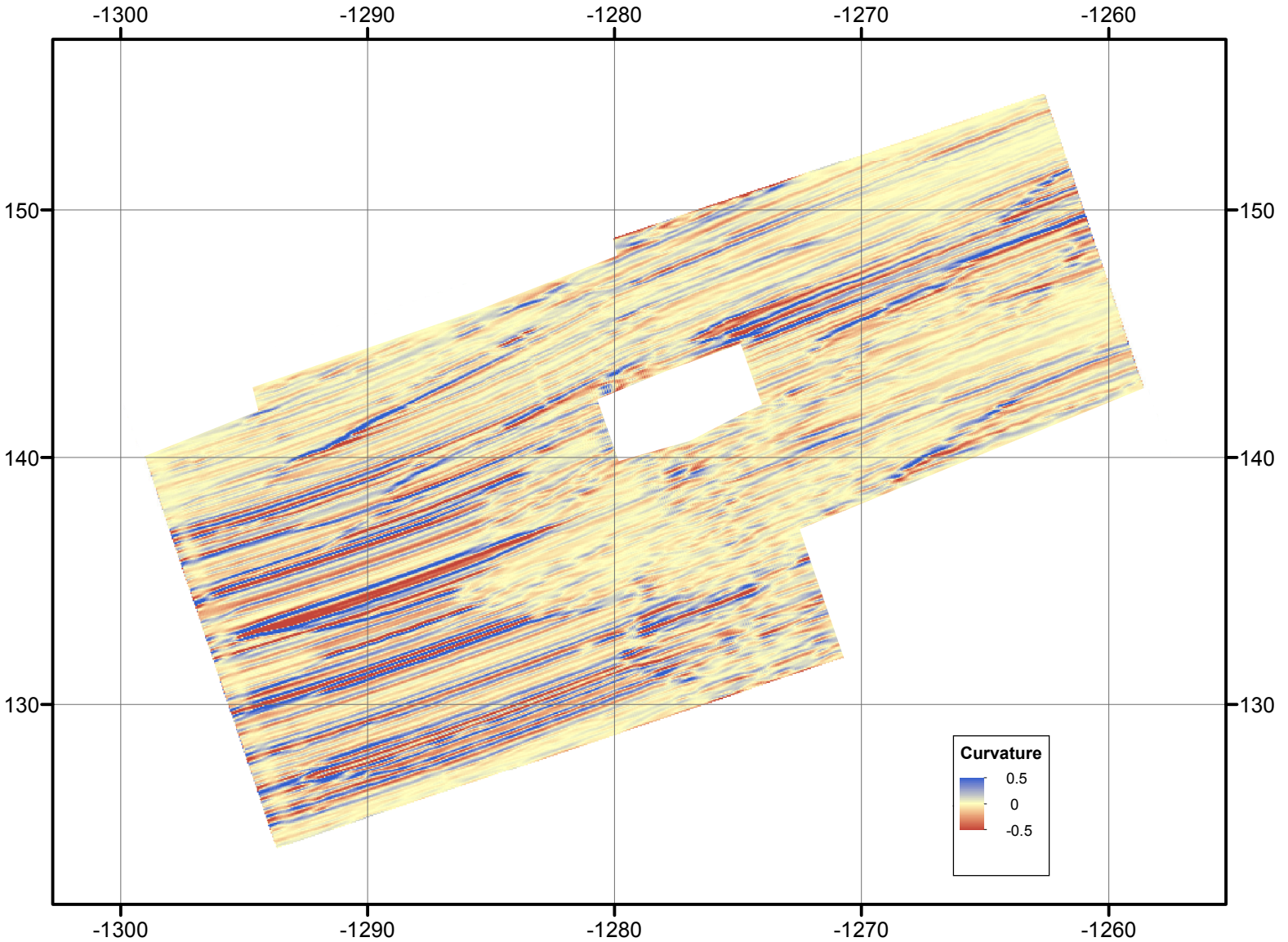

King et al Figure 5

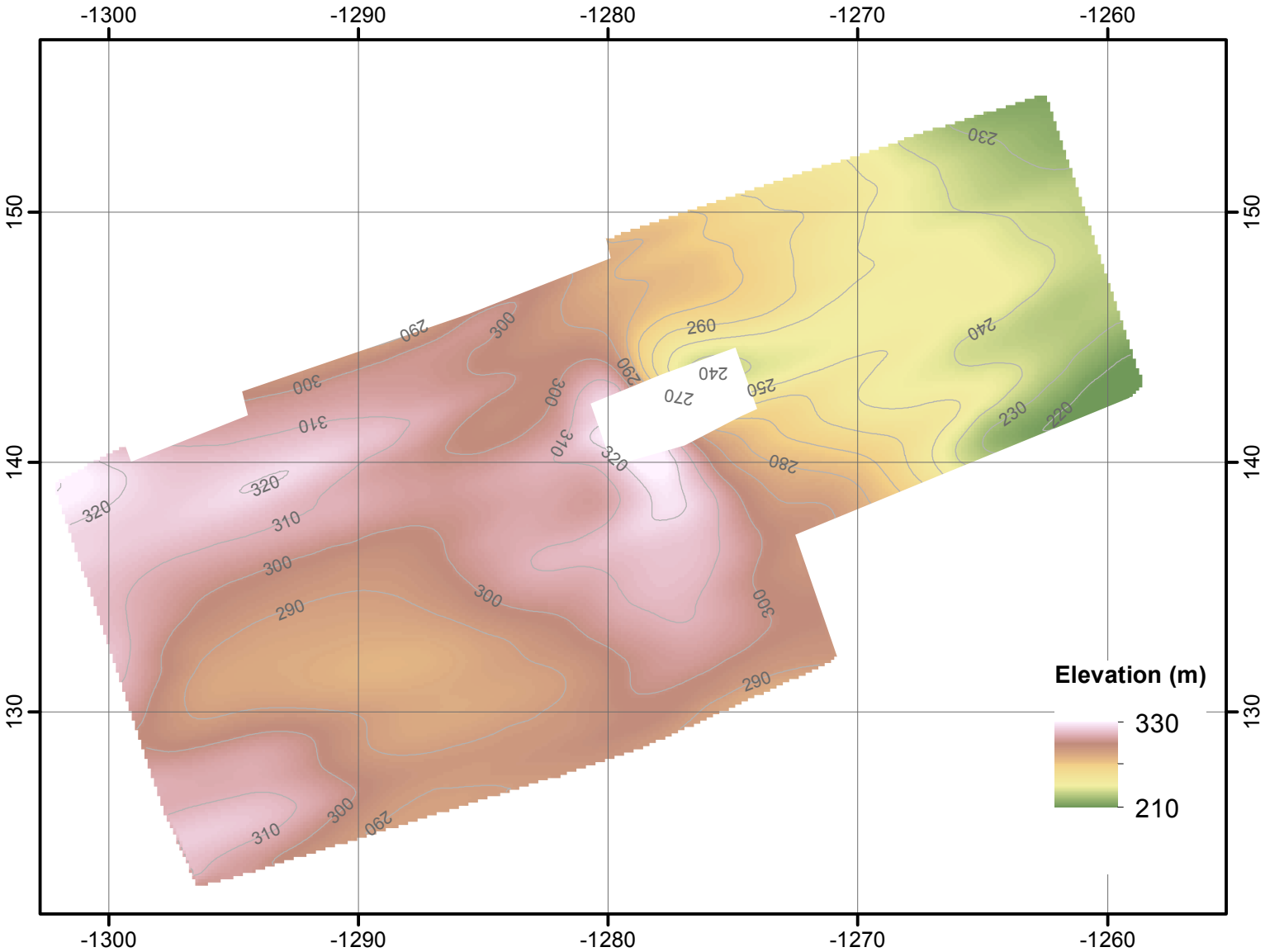

King et al Figure 6

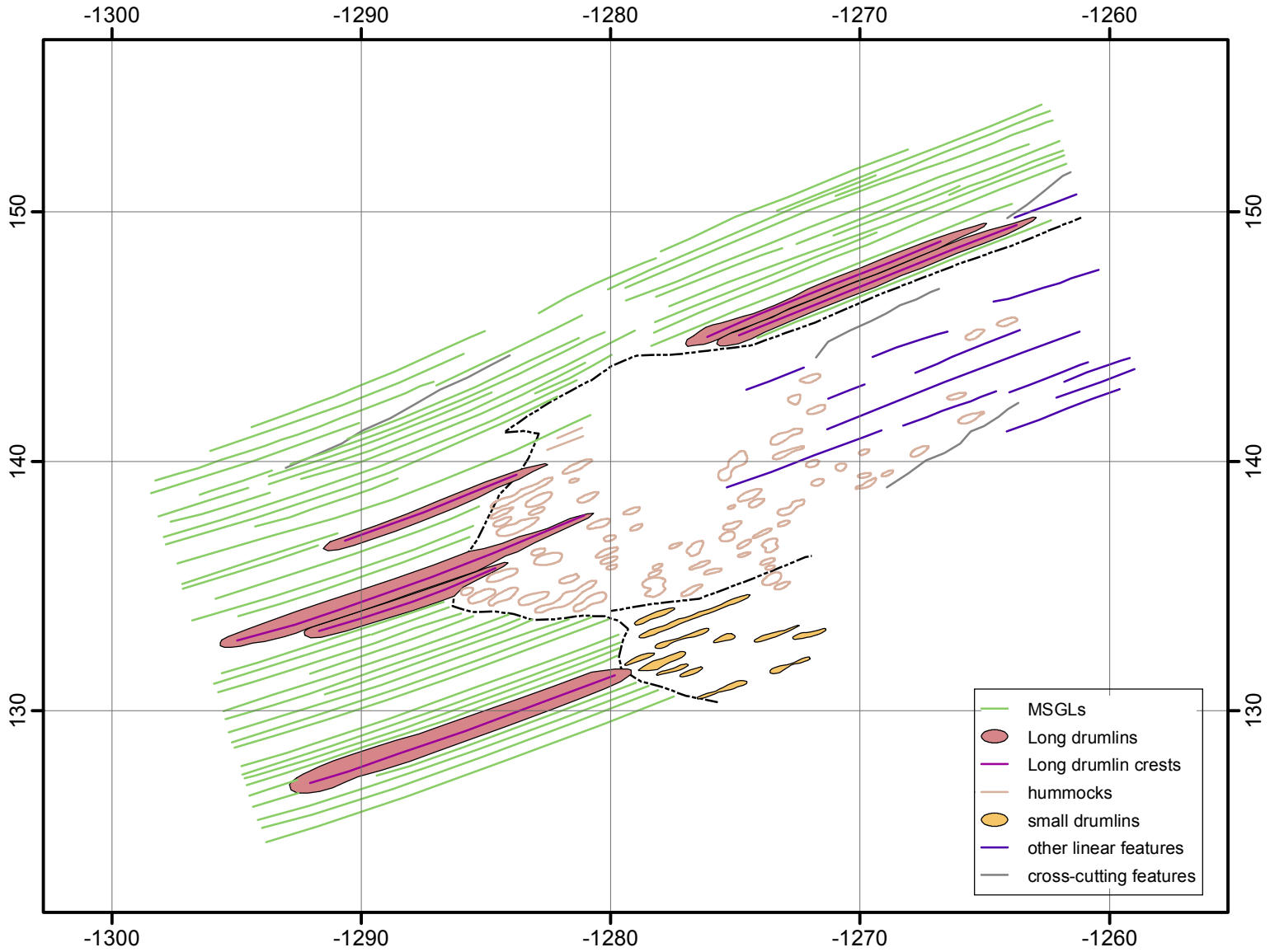

King et al Figure 7

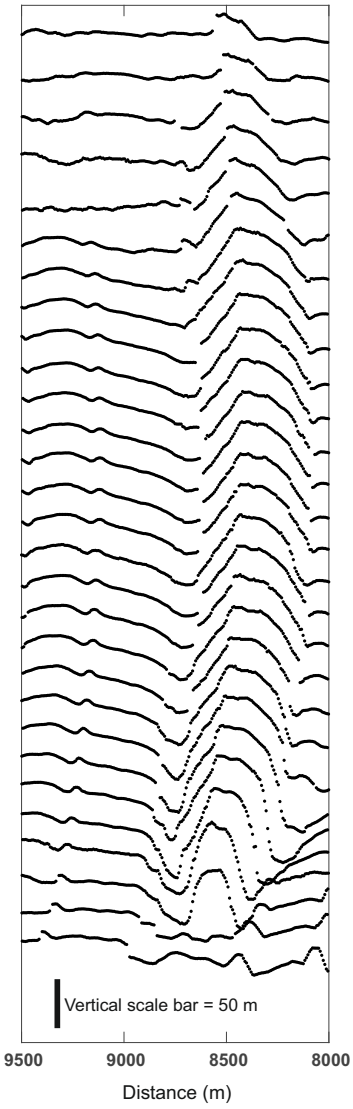
Vertical scale bar = 50 m
9500
9000
8500
8000
Distance (m)

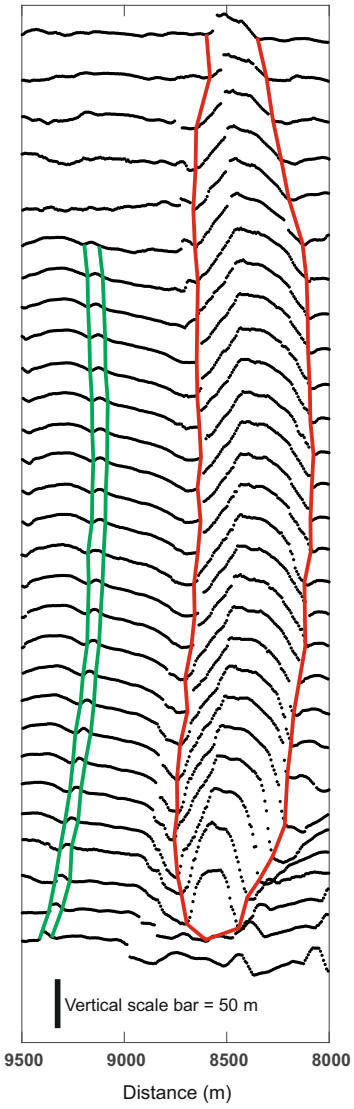
Vertical scale bar = 50 m
9500
9000
8500
8000
Distance (m)